Nucleic Acids Research Advance Access published September 25, 2006

Nucleic Acids Research, 2006, Vol. 00, No. 00 ***e1–9***
doi:10.1093/nar/gkl639

Nanoliter high throughput quantitative PCR

Tom Morrison, James Hurley, Javier Garcia, Karl Yoder, Arrin Katz, Douglas Roberts, Jamie Cho, Tanya Kanigan, Sergey E. Ilyin[1], Daniel Horowitz[1], James M. Dixon[1] and Colin J.H. Brenan*

BioTrove Inc., 12 Gill Street, Suite 4000, Woburn, MA 01810, USA and [1]Johnson & Johnson Pharmaceutical Research & Development, LLC, Spring House, PA 19477, USA

Received June 15, 2006; Revised and Accepted August 16, 2006

ABSTRACT

Understanding biological complexity arising from patterns of gene expression requires accurate and precise measurement of RNA levels across large numbers of genes simultaneously. Real time PCR (RT-PCR) in a microtiter plate is the preferred method for quantitative transcriptional analysis but scaling RT-PCR to higher throughputs in this fluidic format is intrinsically limited by cost and logistic considerations. Hybridization microarrays measure the transcription of many thousands of genes simultaneously yet are limited by low sensitivity, dynamic range, accuracy and sample throughput. The hybrid approach described here combines the superior accuracy, precision and dynamic range of RT-PCR with the parallelism of a microarray in an array of 3072 real time, 33 nl polymerase chain reactions (RT-PCRs) the size of a microscope slide. RT-PCR is demonstrated with an accuracy and precision equivalent to the same assay in a 384-well microplate but in a 64-fold smaller reaction volume, a 24-fold higher analytical throughput and a workflow compatible with standard microplate protocols.

INTRODUCTION

Central to research into cell survival, growth and differentiation in normal and diseased states is the ability to quantify altered patterns of gene expression. Oligonucleotide (1,2) and cDNA (3) hybridization microarrays have emerged as the leading quantitative tool for analyzing transcription of many thousands of genes in a sample simultaneously (4) yet have known limitations in analytical performance and sample throughput (5–7). Real time or quantitative polymerase chain reaction (qPCR) (8) is the superior alternative because of its high accuracy, precision and dynamic range and, as a consequence, is the reference assay for calibration and validation of microarray data (9). However, scaling qPCR to analyze larger numbers of genes and samples simultaneously is intrinsically prohibited by the logistics and cost of the assay in its current microliter format in 96- or 384-well microplates.

High throughput PCR strategies have focused on smaller reaction volumes and follow one of two fluidics methods. Fast sequential analysis is exemplified by monolithic, functionally integrated lab-on-a-chip devices that flow a sample bolus through fixed temperature zones of a micromachined channel for target sequence PCR amplification, followed by sequence specific capture by hybridization and electrochemical detection (10), fluorescence detection (11) or electrophoretic separation with fluorescent detection (12). With quantitative performance similar to a microarray, detection sensitivity is further constrained by sample throughput and the increased potential for cross-contamination from processing samples in a common microchannel.

Many of these problems are mitigated in a parallel fluidics approach. Miniaturized versions of microplates based on high-density arrays of wells etched in a planar substrate is the basis for nanoliter- (13–16) or picoliter-scale PCR (17) in an array format. Other embodiments include PCR in microdroplets on a patterned hydrophobic–hydrophilic surface (18) or in a 2D array of communicating microchannels (19–21). Reports of quantitative nucleic acid measurement in these devices have focused on limiting dilution schemes (22–24), which is clearly not high-throughput. Achieving high areal densities of physically independent reaction containers (>4/mm^2) requires stringent fluidic isolation between adjacent containers and a high degree of environmental control to prevent cross-contamination and evaporative loss during temperature cycling. Despite these challenges, parallel micro- or nanofluidics offers throughput advantages by thermal cycling and imaging many reactions at once to quantify target copy number in multiple genes and samples, simultaneously. Imaging reactions in parallel allows for longer integration times, improves detected signal-to-noise ratios and benefits PCR specificity and sensitivity by requiring fewer temperature cycles to detect a given target copy number. Shorter cycle times are facilitated by rapid heat transfer across proportionally larger surface areas as the reaction volume is reduced.

*To whom correspondence should be addressed. Tel: +1 781 721 3615; Fax: +1 781 721 3601; Email: cbrenan@biotrove.com

Intuitively, an approach to high-throughput qPCR grounded in a high-density array of nanoliter reactions is attractive because it combines the high precision, accuracy and dynamic range of qPCR with the parallelism of a microarray for simultaneous quantification of gene expression across multiple genes and samples. For this to occur, two challenges need to be overcome. The first is creation of a simple interface for precise and accurate transfer of liquids between the wells of a microplate to those of a nanoplate. The second is achieving the accuracy, precision and sensitivity demanded by qPCR in a 96- or 384-well microplate but in a substantially reduced reaction volume. Discovery of a facile interface for speedy transfer of liquids between micro- and nanoplates and identifying a robust approach to ensure qPCR assay performance at the nanoliter-scale has been at the leading edge of our development efforts.

We have solved these problems with an approach based on through-hole arrays (25–27). Effectively thought of as a high-density version of a microplate, our nanoplates combine the high-throughput and reagent savings of a nanofluidic system with the macroscale performance of qPCR in microplates. A stainless steel (317 stainless steel) platen the size of a microscope slide (25 mm × 75 mm × 0.3 mm) is photolithographically patterned and etched to form a rectilinear array of 3072, 320 μm diameter through-holes. The through-holes are grouped in 48 subarrays of 64 holes each and spaced on a 4.5 mm pitch equal to that of wells in a 384-well microplate (Figure 1). A series of vapor and liquid deposition steps covalently attaches a PCR compatible polyethylene glycol (PEG) hydrophilic layer amine-coupled to the interior surface of each through-hole, and a hydrophobic fluoroalkyl layer to the exterior surface of the platen. The differential hydrophilic–hydrophobic coating facilitates precise loading and isolated retention of fluid in each channel. Primer pairs stored in 384-well microplates are transferred into individual through-holes by an array of 48 slotted pins manipulated by a 4-axis robot (*XYZθ*) in an environmentally controlled chamber to prevent evaporative loss during loading. Once a platen is fully populated with primer pairs, the solvent is evaporated in a controlled manner leaving the primers immobilized in a PEG matrix on the inside surface of each through-hole. The array loaded with primer is stored in an evacuated Mylar™ bag at −20°C, ready for sample addition.

Up to 48 different, previously prepared cDNA samples at a concentration of 32 ng/μl are mixed with off-the-shelf qPCR reagents for SYBR Green PCR (see Materials and Methods; PCR Mix) and dispensed into each sub-array (one sample per sub-array) with an automated 48 pipette tip dispensing device. A slotted cassette for holding the platen is assembled by sandwiching a U-shaped glass-reinforced epoxy polymer spacer between two microscope slides patterned with an opaque ink to optically mask background autofluorescence from the spacer. A degassed, immiscible perfluorinated liquid (Fluorinert™) is dispensed into the cassette, the platen inserted and the assembly hermetically sealed with a plug of ultraviolet (UV) curable epoxy.

Real time PCR (RT-PCR) occurs in a computer-controlled imaging thermal cycler whose essential components are two pairs of off-axis, high energy light emitting diode (LED) excitation sources, a thermoelectric flat block holding up to three encased arrays, two emission filters in a computer-controlled filter wheel and a thermoelectrically-cooled CCD camera. Under software control, the real time method for 9216 PCR amplifications and dissociation curves is implemented in <4 h. Post-acquisition data processing generates fluorescence amplification and melt curves for each through-hole in the array, from which cycle threshold (C_T) and melt temperature (T_m) are computed. All data are stored in a flat file (*.csv) format for ready export to a database or third party software for further analysis.

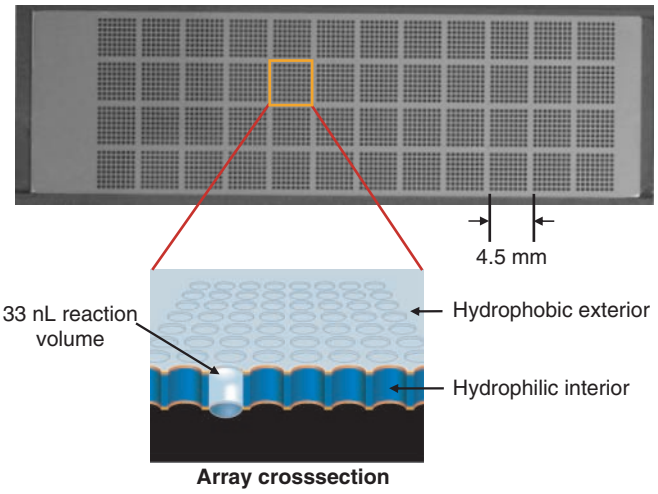

Figure 1. A stainless steel platen (317 stainless steel) the size of a microscope slide (25 mm × 75 mm × 0.3 mm) is photolithographically patterned and wet etched to form a rectilinear array of 3072 micro-machined, 320 μm diameter holes of 33 nl each. The 48 groups of 64 holes are spaced at 4.5 mm to match the pitch of the wells in a 384-well microplate. A PCR compatible PEG hydrophilic layer is amine-coupled to the interior surface of each hole and a hydrophobic fluoroalkyl layer is vinyl-coupled to the exterior surface of the platen, resulting in the retention in individual, isolated containers of PCR reagents and sample introduced onto the array.

MATERIALS AND METHODS

Through-hole array fabrication

Sheets comprised of 12 arrays attached by thin tabs to a support frame were purchased from Tech-Etch Inc. (Plymouth, MA). The arrays are fabricated by double-sided wet-etching of a photolithographically-patterned 300 μm sheet of 317 stainless steel resulting in the hole pattern shown in Figure 1. The sheets are cleaned for 2 h in 10% RBS 35 (Pierce) at 50°C, rinsed in reverse osmosis de-ionized (RODI) salt water and dried with a stream of dry nitrogen gas. A vinyl-terminated silane monolayer (7-octenyltrimethoxysilane, Gelest) is vapor deposited [5 h, 100°C in a vacuum oven (VWR)] followed by a 30 min NH_3(g) cure.

Next, the vinyl groups inside the through-holes are selectively oxidized by first immersing the sheet in a 1l bath of ethanol to overcome the surface tension of the hydrophobic coating followed by immersion in 1L of RODI water. The sheet is next slowly passed through a layer of 30 ml of an oxidation solution (5 mM $KMnO_4$ and 19.5 mM $NaIO_4$) floating on 1l of Fluorinert™ (FC3283), incubated for 2 h, rinsed in RODI water and dried in a stream of dry nitrogen gas.

After oxidation, a hydrophilic PEG layer is deposited inside the through-holes by repeating the previous steps except replacing the oxidation solution with 30 ml of 15 mg/ml EDC (Pierce) and 5 mg/ml PEG 5000 (Nektar-Synasia) in HEPES buffer (pH 7.5). After incubation for 2 h, the sheet is removed and dried overnight at 100°C under vacuum. A second hydrophobic layer is added by vapor deposition of heptadecafluorotriethoxysilane (Gelest) for 2 h, 150°C in a vacuum oven followed by a 30 min cure with NH_3(g). Finally, the array sheets are rinsed in RODI water to remove the physisorbed PEG layer, thus exposing the underlying covalently linked hydrophilic PEG.

cDNA preparation

RNA samples were converted to randomly primed first strand cDNA using High Capacity cDNA Archive Kit (Applied BioSystems, Foster City, CA). To reduce non-specific product formation during qPCR, the cDNA sample was heated to 75°C for 10 min to inactivate the reverse transcriptase; snap chilled on ice for 5 min, then treated 1 h with 1.3 U/μl Exonuclease I (Amersham Biosciences, Piscataway, NJ). The Exonuclease I is heat inactivated at 85°C for 10 min and the resulting cDNA solution is stored at −20C.

PCR mix

The PCR master mix consists of 1× LightCycler™ FastStart DNA Master SYBR Green I (Roche Applied Science, Indianapolis, IN), 0.2% (w/v) Pluronic F-68 (Gibco, Carlsbad, CA), 1 mg/ml BSA (Sigma–Aldrich, St. Louis, MO), 1:4000 SYBR Green I (Sigma–Aldrich), 0.5% (v/v) Glycerol (Sigma–Aldrich), 8% (v/v) Formamide (Sigma–Aldrich) and sample. For each kinase test of 507 assays, 66 μl of reaction mix was required.

Primer design

Kinase genes were selected based on their classification in Gene Ontology (www.geneontology.org) and their presence in the RefSeq database (www.ncbi.nlm.nih.gov/RefSeq). Primer pairs biased towards the 3′ end of these genes were obtained from either PrimerBank (28) and http://pga.mgh.harvard.edu/primerbank or designed using Primer3 [http://frodo.wi.mit.edu/cgi-bin/primer3_www.cgi]. Primers were ordered from a commercial supplier (Sigma-Genosys, www.sigma-genosys.com) and their performance was validated with the following process. An ABI 7900 (Applied BioSystems Inc., Foster City, CA) was used to test if each primer set run against either five tissue cDNA library (qPCR Human Reference cDNA, BD BioSciences, Franklin Lakes, NJ) or 37 tissue cDNA library (BD Quick-Clone II Human Universal cDNA, BD BioSciences, Franklin Lakes, NJ) could generate a product rising above 0.2 ΔR_n. Amplicon mobility in 4% agarose E-gels (Invitrogen, Carlsbad, CA) was measured from images captured with a gel imager (AlphaImager, AlphaInnotech, San Leandro, CA) and processed by software (Quantity One 1-D Analysis Software; BioRad, Hercules, CA) to confirm the primer set made a product within 10% of the predicted length. Amplicons generated from primer pairs passing the above criteria were pooled and gel purified to remove fragments <80 and >400 bp in size. This pool was used as a source of template in subsequent PCR array validation experiments. All amplicons were sequenced; ∼70% matched all or part of the expected target sequence while although the remainder could not be confirmed by sequencing, these amplicons nonetheless matched the expected size of the predicted amplified product.

Primer validation

The primer concentration where each primer set fails to produce a product in the PCR array was determined. The working primer concentration was adjusted to 8-fold above this concentration to ensure that small quantities of primer carryover between holes during sample loading will reduce interference with PCR in adjacent holes. Assays were demonstrated to have at least a 95% confidence of detecting 4-fold change at >100 copies by first measuring a <0.5 C_T STD across greater than five replicates and then demonstrating a ΔC_T shift of 2 +/−1 cycle for a sample diluted 4-fold. The template for these experiments was the pooled amplicon template in 1 ng total RNA equivalent randomly primed liver cDNA, with an average of 200 +/−100 starting copy number. A pass rate of 60% was observed with this validation process.

Real time thermal cycler protocol

The PCR array thermal cycling protocol consisted of 10 min, 92°C polymerase activation step followed by 35 cycles of 15 s @ 92C, 1 min @ 55°C and 1 min @ 72°C (imaging step). Following amplification, amplicon dissociation was measured by cooling the PCR array to 65°C then slowly heated to 92°C @ 1°/min, with images collected every 0.25°C.

Human umbilical vein endothelial cells (HUVEC sample preparation

Pooled HUVEC and Endothelial Cell Medium-2 (EGM(tm)-2) were purchased from CAMBREX BIO SCIENCE (Walksersville, MD). Recombinant Human TNF-α (10 ng/ml in EGM™-2), purchased from R & D Systems Inc. (Minneapolis, MN) was added to HUVEC cultures that were ∼50% confluent in T150 tissue culture flasks. Cultures were incubated for 4 h at 37C, 5% CO_2. Medium was removed and 2.5 ml of TRI Reagent® (Molecular Research Center) was added to lyse cells. RNA was purified using an RNeasy Mini Kit (Qiagen Inc.) and reverse transcription was done using a High Capacity cDNA Archive Kit (Applied Biosystems). Samples were treated with Exonuclease I (10 U/μl) (Amersham Biosciences).

RESULTS

Baseline qPCR performance: uniformity, precision, accuracy, sensitivity and dynamic range

To examine amplification uniformity, three arrays were uniformly loaded with PCR mastermix, *CycA* primer pairs and amplicon, resulting in an average of 500 starting copies of amplicon per through-hole. OD_{260} of purified amplicon was used to independently confirm the number of starting copies per hole. An image generated by subtracting pixel values of the first and 19th cycling image (Figure 2A) provides a visualization of amplicon replication in each

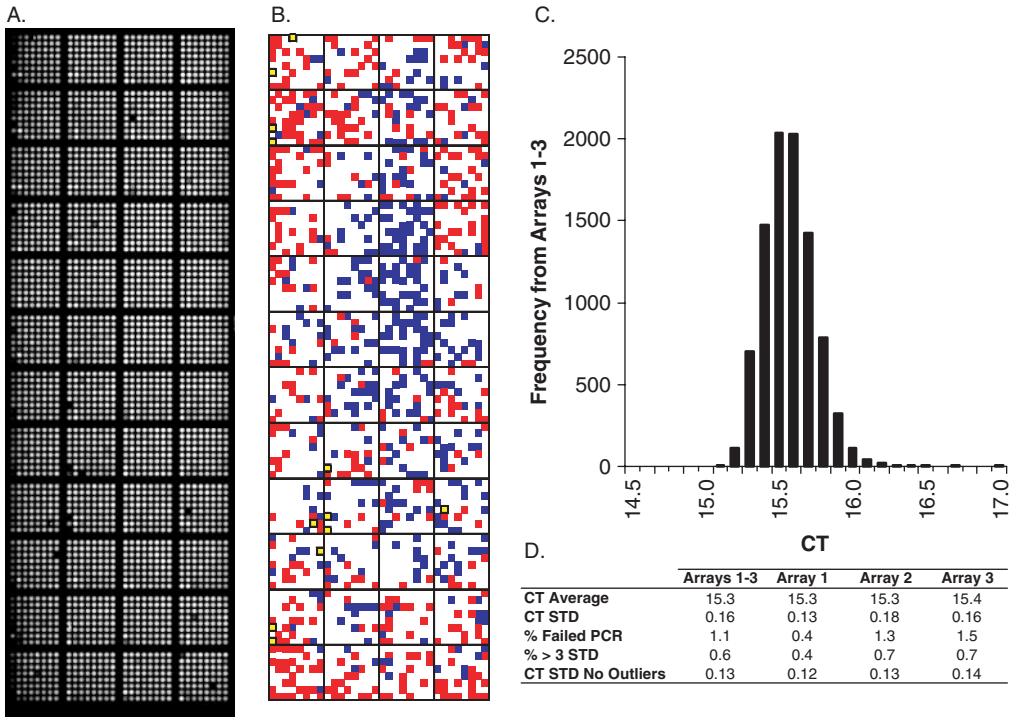

D.

	Arrays 1-3	Array 1	Array 2	Array 3
CT Average	15.3	15.3	15.3	15.4
CT STD	0.16	0.13	0.18	0.16
% Failed PCR	1.1	0.4	1.3	1.5
% > 3 STD	0.6	0.4	0.7	0.7
CT STD No Outliers	0.13	0.12	0.13	0.14

Figure 2. Three through-hole arrays were loaded with PCR reagents containing 500 starting templates per hole and subjected to 32 cycles of PCR. The amplicon product image (**A**) was generated by pixel-by-pixel subtraction of cycle image 1 from 19 for Array 1. The C_T color map for Array 1 (**B**) indicates holes within C_T 1 STD from average (white), C_T < average −1 STD (blue), C_T > average +1 STD (red) and failed reactions (yellow). C_T distribution plot (**C**) for all three arrays, and performance specifications table (**D**) for each array analyzed either independently or combined, summarize the instrumentation uniformity results.

through-hole of the array. Dark holes resulting from a sample loading failure are detected by the absence of SYBR Green fluorescence. Fluidics errors are typically <2% and are stochastically distributed amongst the through-holes as failed PCRs (Figure 2B). The dimmer holes along the first and last column of the array image are not from reduced yield of PCR product but rather from reduced SYBR fluorescence intensity from non-uniformities in LED excitation, imaging field of view and slight variations in optical path at the refractive index boundaries across the array. These fluorescent signal differences (≈6% CV, data not shown) are corrected for in the instrument calibration. Residual optical differences are taken into account by fluorescent baseline normalization of the amplification curve for each through-hole prior to crossing threshold (C_T) calculation. The mean C_T for 500 starting copies is 15.3 cycles, on average about 11 cycles earlier than microplate-based qPCR systems. The C_T shift results from a higher concentration of amplified products expected for PCR at reduced volumes (22) and an improved C_T calling algorithm we developed by combining baseline intercept with numerical modeling of the exponential amplification phase. The instrument precision at 500 starting copies was +/−0.16 C_T (or <12% CV on copy number), estimated from the C_T STD for >9100 amplification reactions (Figure 2D). The C_T distribution (Figure 2C) follows a Gaussian distribution slightly skewed towards delayed (higher) C_T and with 0.6% of the through-holes having outlier C_Ts > 3 STD from the mean. While the C_T map (Figure 2B) indicates a small C_T gradient spanning 0.32 cycles diagonally from the middle of the array, outliers map stochastically (data not shown). We speculate that the reduced PCR efficiency of the outlier population may arise from random micro-scale defects of the interior polymer surface coating and/or contamination by random interfering particulates, but their impact on data quality is substantially reduced with replicate assays.

PCR array thermal uniformity was examined by melt curve analysis of the amplicon products shown in Figure 3. Following PCR, the array temperature was equilibrated to 65C, slowly ramped to 92°C at 1°C per minute, and SYBR Green fluorescence images were collected every 0.25°C to record SYBR Green dye quenching on amplicon dissociation. The product melt temperature, T_m, for each through-hole is derived as the maximum of $-dF/dT$, where T is the array temperature and F is the fluorescence emission from a through-hole at each temperature (29). The T_m distribution across the PCR array (Figure 3A) indicates the array center was 1° cooler than at its edge. The T_m computed across three arrays produced a similar T_m distribution (Figure 3B) and mean T_m, with an array-to-array T_m STD equal to ±0.28°C (Figure 3C).

The dynamic range and accuracy of the instrument was measured by performing RT-PCR on a *CycA* amplicon titration. Figure 4A depicts 12 replicate amplification profiles for each log dilution, ranging from 10^7 to 1 starting copies per hole and a no template control. The high quality curves showed >150-fold signal-to-noise, and >4 cycles exponential-phase amplification. The C_T computed from these curves were linear

over 6 log amplicon concentrations (Figure 4B, $R^2 = 0.99$), and near perfect amplification efficiency based on slope of C_T versus log starting copy plot. The precision for measurements $\geqslant$1000 starting copies was equivalent to the earlier PCR uniformity experiment, averaging around 0.17 STD C_T. The no template control had no detectable product, indicating carryover between subarrays is below the limit of detection.

Sensitivity can be estimated by measuring the frequency of PCR positive reactions near the limit of assay detection. The decreasing precision below 1000 copies appears to follow the noise contribution based on the Poisson effect (Figure 4B). Holes predicted to have an average of a single starting copy produced 49 of 64 positive assays (77%); reasonably close to the 63% predicted by Poisson statistics. Taken together, the through-hole array demonstrated single copy sensitivity. Additional thermal cycling of these arrays show no increase in assay positive holes, indicating that there is no intra subarray carryover of primers at the level of single copy sensitivity.

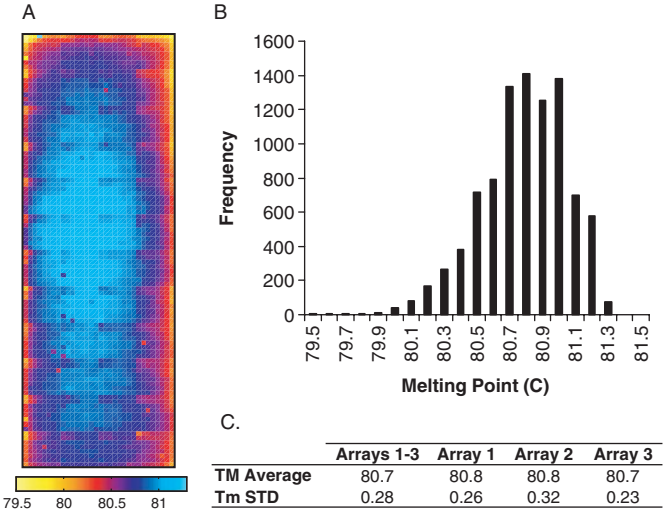

C.

	Arrays 1-3	Array 1	Array 2	Array 3
TM Average	80.7	80.8	80.8	80.7
Tm STD	0.28	0.26	0.32	0.23

Figure 3. Following 32 cycles of PCR, the arrays in Figure 2 were cooled to 65°C then slowly heated to 92°C at 1 C/min. A dissociation curve (F versus T) and T_m $[(-dF/dT)_{max}]$ was calculated for each sample from fluorescent images collected every 0.25C. The heat map (**A**) for Array 1 indicates T_m spanning 79.5°C (yellow) to 81.3°C (light blue). Plot (**B**) indicates the T_m distribution for all three arrays and Table (**C**) breaks down the T_m performance either independently or combined.

qPCR measurement of differential expression of human kinase genes between human heart and human liver RNA samples

To assess the performance of the system with a biologically relevant example, an array was constructed with primer pairs targeting expression of 508 human kinases, 13 endogenous (housekeeping) controls in quadruplicate and 208 negative controls for analyzing four samples per array (see Materials and Methods, Primer Validation). Normal human heart and liver RNA from a commercial source was reverse transcribed into cDNA equivalent and divided into two aliquots of 0.25 and 1 ng cDNA per through-hole. The pipette sample loader transferred sample mixed with PCR mastermix into arrays pre-loaded with the assay primer sets and the arrays were processed according to the real time procedure described in the Methods section.

Correlation of C_T technical replicates for the heart (Figure 5A) and liver (Figure 5B) samples at 1 and 0.25 ng of cDNA per through-hole shows high assay precision and accuracy across a large dynamic range of responses. With 1 ng cDNA per through-hole, 78% of the assays for the heart sample have STD <0.5 while for liver, 72% of the assays had this precision or better (Figure 5C). Assay accuracy was estimated from computing the mean C_T difference between two different cDNA concentrations for the heart and liver samples. A histogram of ΔC_T for all assays in both tissues shows a median C_T of 1.8 ± 0.48 for heart and 1.7 ± 0.61 for the liver sample, indicative of a 4-fold change in cDNA concentration. Negative controls in each subarray

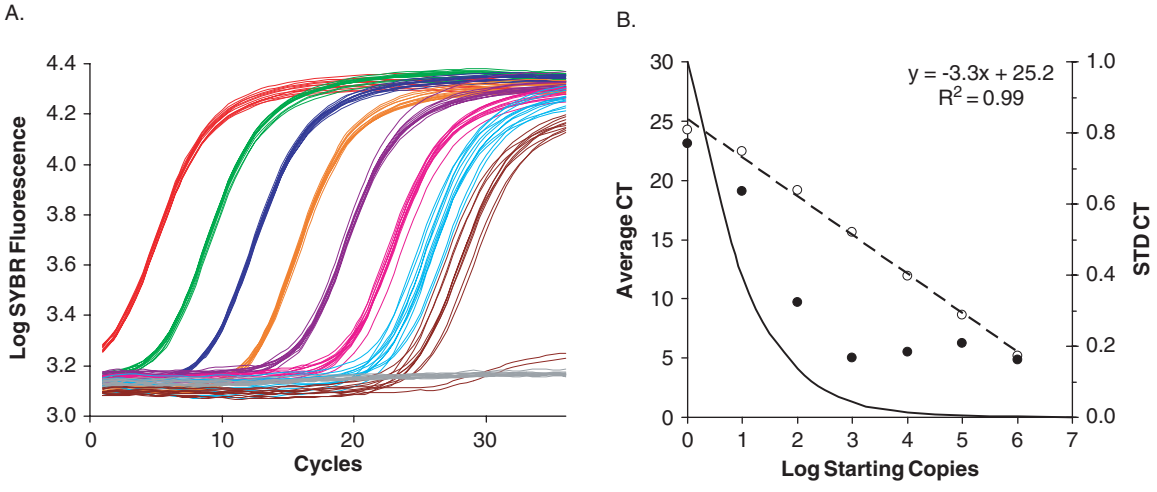

Figure 4. qPCR Titration Curve. (**A**) depicts cycle-by-cycle log SYBR fluorescence of each through hole colored according to average starting amplicon copy per hole [10^7 to 1 plus no template control (gray), 12 of the 64 replicates depicted]. (**B**) indicates average C_T (open circles) and STD C_T (filled circles) plotted against log starting copies ($n = 64$); line formula and Pearsons Coefficient were calculated from dashed C_T curve. Predicted Poisson noise is indicated by the solid curve.

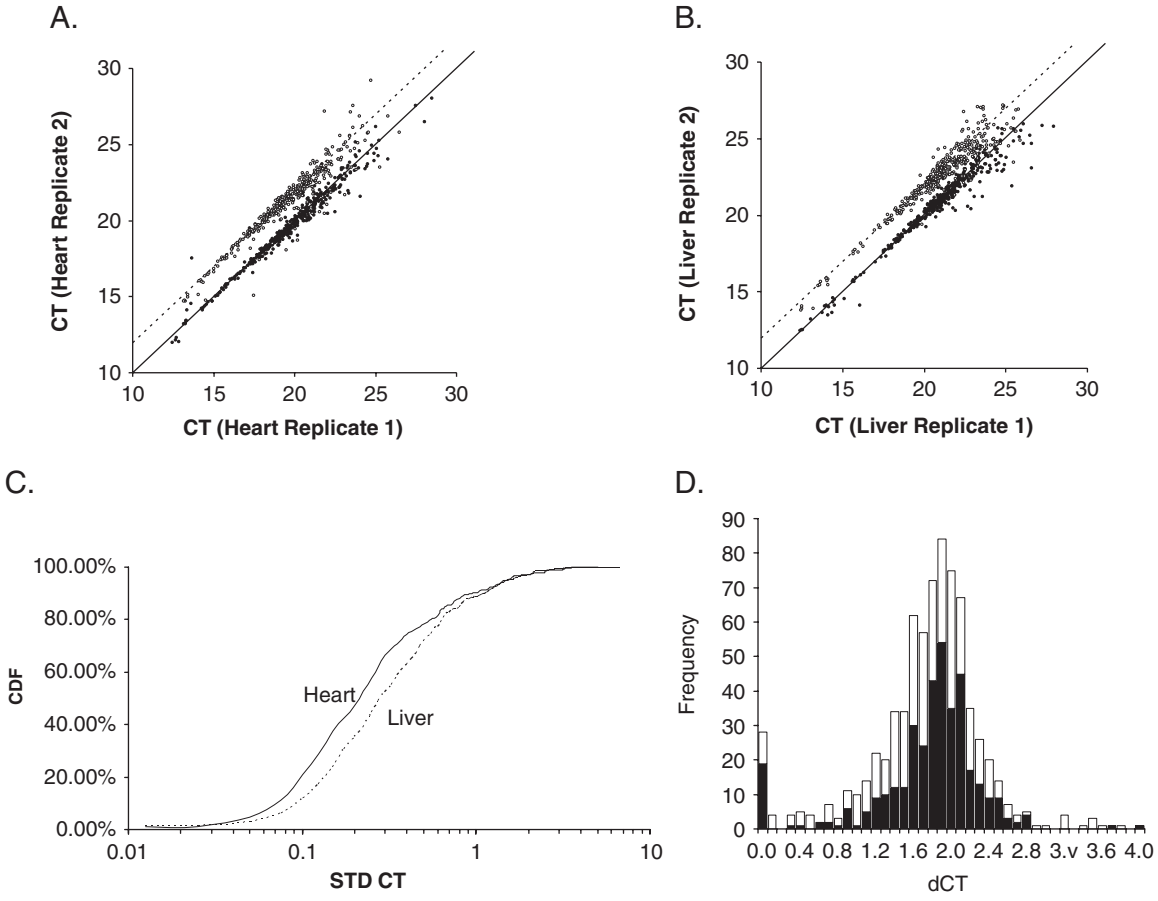

Figure 5. Human heart and liver differential kinase gene expression. A Gene Ontology database was used to select 507 human kinase genes along with 13 housekeeping genes. Primers were designed, loaded into a through-hole array and SYBR Green PCR was used to measure transcript levels of normal human liver (**B**) or heart (**A**) samples. Replicate 1 samples were at 1 ng/hole, whereas replicate 2 samples were at either 1 ng/hole (filled circles) or 0.25 ng/hole (open circles). The solid diagonal lines represent 1:1 correlation for 1 ng cDNA/through-hole, and the dashed line the 1:1 correlation for 0.25 ng cDNA/through-hole. The cumulative distribution of assay standard deviation at 1 ng/hole for both liver and heart samples (**C**) shows over 70% of the assays have a precision <0.5. ΔC_T for the difference in sample assay pair (Replicate 2–Replicate 1) is represented in histogram (**D**), liver indicated by unfilled bars and heart indicated by filled bars.

showed no detectable carry-over between through-holes (0/1728 negative controls).

Differential gene expression between the heart and liver samples at 1 ng cDNA per through-hole was determined by comparing the difference in mean C_Ts for each gene in the liver and heart assay populations (Figure 6A). Positive assays for which an accurate C_T could be measured passed the following criteria: (i) the amplicon product was detected and confirmed by melt curve analysis; (ii) target expression greater than single copy in both tissues (CT < 25) and (iii) each assay had a technical replicate $\geqslant$2. Eighty-three assays were rejected based on these criteria and the remaining 442 positive assays were normalized relative to the geometric mean of the same 13 housekeeping genes for each tissue. Two subpopulations are observed when the difference in expression for the same gene is compared between the two tissues: (i) tissue-specific expression where the gene expressed at less than 10 copies in one tissue but not the other and (ii) the gene expressed in both tissues with an abundance >10 copies but there is a significant difference in expression between the tissues based on Student's *t*-test (two-tailed distribution and two-sample unequal variance) with a *P*-value <0.005. Segmentation of the assay population based on these criteria is not surprising given the physiological differences between heart and liver tissue, even for common functional pathways.

Consider the well-studied glycolysis pathway as a point of comparison where multiple kinases play fundamental roles in the multi-step oxidation of glucose to pyruvate and ATP (30). The first step in this process is ATP-dependent phosphorylation of glucose to the intermediate glucose-6-phosphate by the liver-specific hexokinase isozyme glucokinase (*GCK*; NM_000162). We detected insignificant expression levels in the heart sample (<1 copy) compared with substantially higher levels in the liver sample (>200 000-fold higher). A similar pattern of tissue-specific expression was recorded for the liver (*PFKL*; NM_002626) and muscle (*PFKM*; NM_000289) isoforms of phosphofructose kinase; and the muscle (*PKLR*; NM_000298) and liver (*PKM2*; NM_002654) isoforms of pyruvate kinase. In contrast, *PGK1* (NM_000291), one of two isoforms of phosphoglycerate kinase, shows a small yet significant difference in expression between the heart and liver sample (4.7-fold; $P = 6 \times 10^{-7}$) yet is expressed at high

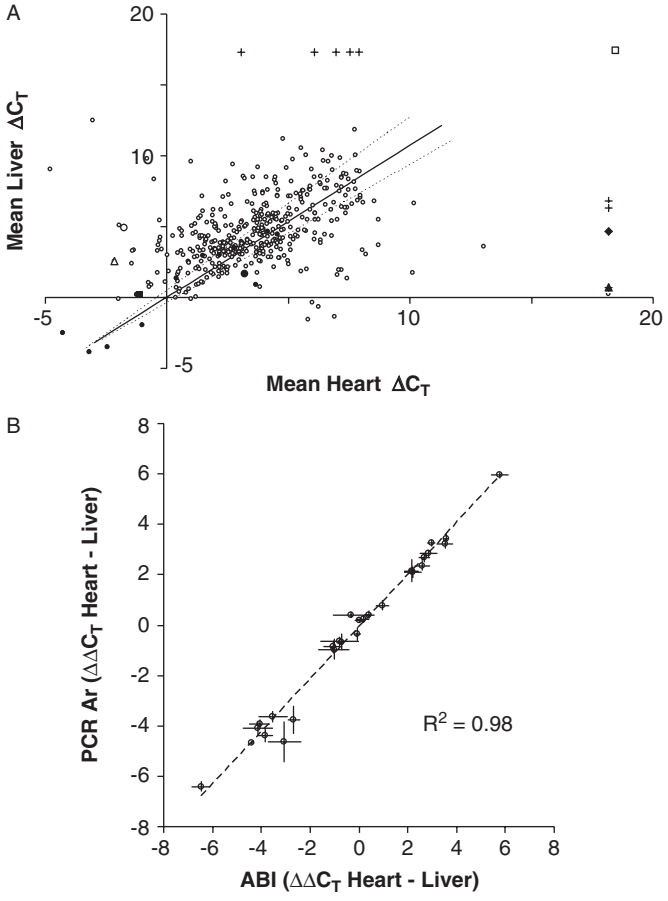

Figure 6. Liver and heart kinase genes differential expression. C_T data from both tissues at 1 ng/hole was normalized relative to the geometric mean of six housekeeping genes; *B2M* (NM_004048), *ACTB* (NM_001101), *EEF1A1* (NM_001402), *HMBS* (NM_000190), *TBP* (NM_003194), *PPIA* (NM_021130) and plotted as $(\Delta C_T)_{Heart}$ versus $(\Delta C_T)_{Liver}$ in (**A**). Open circles are DC_T measurements ($n = 3$ replicates) and solid circles are housekeeping genes normalizing dataset ($n = 4$ replicates). Error lines (dashed lines) are STD compared with linear fit to housekeeping genes (solid line, $R^2 = 0.99$). Genes with tissue-specific expression ($C_T \geq 20$ in one tissue, $C_T < 20$ in the other tissue) are indicated by crosses. Expression of individual genes are indicated as follows: *GCK* (filled diamond), *PGK1* (filled square), *PGK2* (open square), *PKLR* (filled triangle), *PKM2* (open triangle), *PFKL* (filled circle) and *PFKM* (open circle). Concordance data (**B**) for 21 transcript assays selected from 7 kinase genes spanning a 4000-fold differential heart and liver expression, along with 12 housekeeping genes, were used to perform microplate qPCR in an ABI 7900 at 3 replicates per sample. Average $\Delta\Delta C_T$ were calculated and compared with the same assays in the PCR array; STD (error bars), and 1:1 correlation (dashed line).

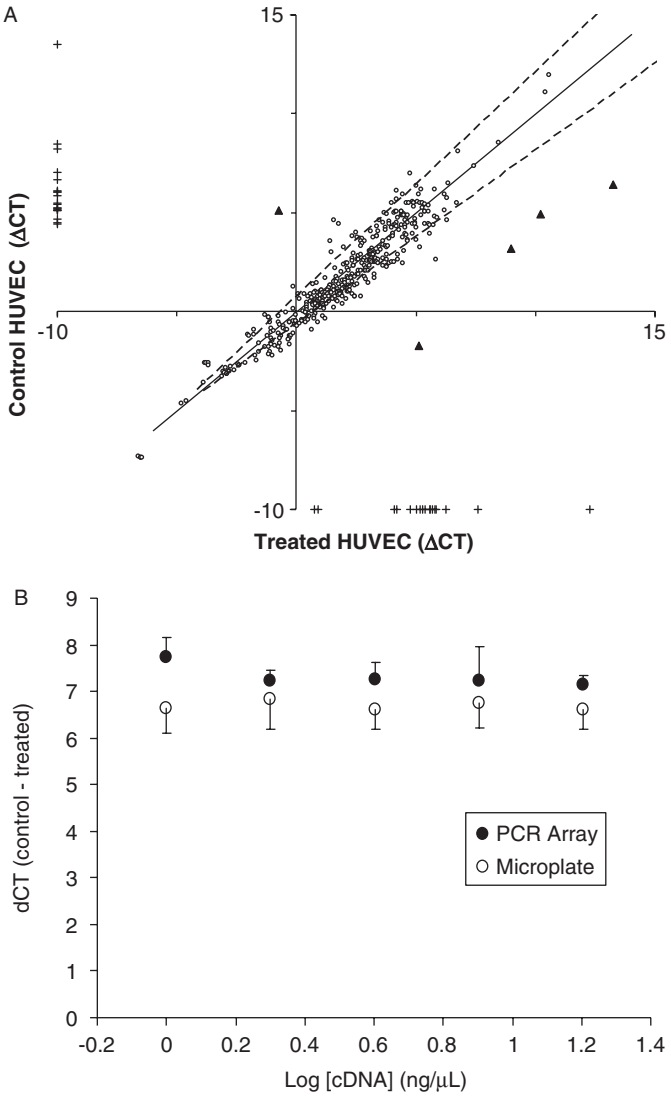

Figure 7. Transcript analysis of TNF-α treated HUVEC. PCR arrays were used to make transcript measurements of cDNA generated from pooled HUVEC cells treated with either TNF-α or vehicle. Samples were normalized (ΔC_T) by subtracting the geometric mean of 13 housekeeping genes from the C_T of each assay. (**A**) Correlates ΔC_T between treated and untreated assays (circles), triangles showing significant difference were, from left-to-right genes *CCL2* (NM_*002982*), *SELE* (NM_000450), *TNFAIP2* (NM_006291), *TNFAIP3* (NM_006290), *VCAM1* ($P < 0.001$, $n \geq 2$ technical replicates) and targets detected in one sample but not the other (pluses). (**B**) Examines fold difference in expression in *SELE* between treated and control HUVEC measured in PCR array and microplate at differing cDNA input quantity (error bars are STD, $n \geq 3$).

levels in both tissues, indicative of its known ubiquitous expression. Expression of the second isoform, *PGK2* (NM_138733), was not detected in either sample; this is not surprising given that *PGK2* is only expressed in meiotic spermatocytes and postmeiotic spermatids during spermatogenesis (31).

To externally validate assay predictions, 21 assays showing higher, equal and lower expression in liver than heart were run in a microplate on a real time thermal cycler (ABI 7900). The resulting measurements showed a high degree of concordance with the PCR array results ($R^2 = 0.98$) with equivalent precision (Figure 6B).

qPCR measurement of differentially expressed genes in TNF-α stimulated NK-β pathway

HUVEC TNF-α response was examined using both a kinase array and a custom array. The custom array contained 26 TNF response pathway assays selected from a library of 2800 validated primer pairs (see Materials and Methods; Primer Validation). The layout of the custom array allows 48 samples per PCR array and the data analysis was similar to the heart-liver comparison. Figure 7A depicts the ΔC_T between the TNF-α treated and vehicle treated HUVEC

(see Materials and Methods). Of the 533 targets screened, 406 were positive in both samples. Negative controls in each sub-array showed no detectable carry-over between through-holes (0/1224 negative controls). As predicted, the TNF-α treatment increased selectin E (*SELE*; NM_000450) and vascular cell adhesion molecule 1 (*VCAM1*; NM_001078) expression level >100-fold (32,33). The dynamic range of *SELE* was compared between microplate and PCR array (Figure 7B) by diluting the sample and determining if the resulting housekeeping-normalized ΔC_T gave the same measurement across the dilution series. The PCR array produced a similar ΔC_T until the *SELE* starting copy number reached single copy in the PCR array hole, ~0.03 ng/hole.

DISCUSSION

A nanofluidic system for performing solution-phase RT-PCR in an array of isolated through-holes overcomes limitations of existing micro- or nanofluidic devices by implementing a parallel approach to fluidic handling that lends itself well to interfacing with microtiter plates for simple and efficacious transfer of liquid samples and reagents into the nanofluidic structure using arrays of slotted pins or pipette tips. The reaction containers are kept separate and distinct by selective and controlled modification of the platen surface to make the inside surfaces of the through-holes chemically distinct from the outside surfaces. In the system described here, the interior surface of each hole is modified to be hydrophilic and the exterior surface hydrophobic.

We validated the system performance by carrying out thousands of real time SYBR Green PCR assays for a number of sample sets. With amplicon as the target, the baseline performance of the system had the same dynamic range, sensitivity and precision as PCR in a microplate but in 64-fold smaller reaction volumes. The increase in C_T variability with decreasing number of target amplicon was shown to follow a Poisson distribution at low copy number, demonstrating the system is capable of single copy detection. Further, the thermal uniformity was demonstrated by the small spread in C_T and T_m in a uniformly loaded array. With volume miniaturization, we identified the need to increase sample concentration to maintain a constant number of target molecules in the reaction volume to obtain the high quality PCR observed.

When challenged with cDNA prepared from normal human heart and liver RNA, the high replicate precision and accuracy enabled detection of tissue-specific expression of kinase genes and discrimination in differential kinase expression between the two tissue types. A large number of genes showed small differences in expression (<2-fold) with a high degree of significance ($P < 0.001$), suggesting the system is potentially capable of revealing new patterns of transcription across large numbers of genes. The data from TNF-α stimulation of the NF-β pathway in HUVEC cells demonstrates this point. The high sample throughput of over 27 000 RT-PCR analyses per person per day, based on a workflow of 3 h to prepare three arrays and three processing runs per day per person, is a 24-fold increase in analytical throughput based on current 384-well microplates and opens new possibilities in genetic system analysis not currently possible. Clearly, the nanofluidic PCR array has the potential to span the space of genomic applications requiring the parallelism of hybridization microarrays with the specificity, accuracy, dynamic range and precision of solution phase PCR.

ACKNOWLEDGEMENTS

The authors wish to thank John Linton, Leila Hasan, Elen Ortenberg, Kevin Pappenfuss, Maria Sousa, Candice Albritton, Mahima Santhanam and Amy Goldberger for their technical assistance. Funding to pay the Open Access publication charges for this article was provided by BioTrove Inc.

Conflict of interest statement. None declared.

REFERENCES

1. Pease,A.C., Solas,D., Sullivan,E.J., Cronin,M.T., Holmes,C.P. and Fodor,S.P. (1994) Light generated oligonuleotide arrays for rapid DNA sequence analysis. *Proc. Natl Acad. Sci. USA*, **11**, 5022–5026.
2. Lipshutz,R.J., Morris,D., Chee,M., Hubbell,E., Kozal,M.J., Shah,N., Shen,N., Yang,R. and Fodor,S.P. (1995) Using oligonucleotide probe arrays to access genetic diversity. *Biotechniques*, **19**, 442–447.
3. Schena,M., Shalon,D., Davis,R.W. and Brown,P.O. (1995) Quantitative monitoring of gene expression patterns with a complementary DNA microarray. *Science*, **5235**, 368–369.
4. Gershon,D. (2002) Micorarray technology: an array of opportunites. *Nature*, **416**, 885–891.
5. Murphy,D. (2002) Gene expression studies using microarrays: principles, problems and prospects. *Adv. Physiol. Educ.*, **26**, 256–270.
6. Petersen,D., Chandramouli,G.V., Geoghegan,J., Hilburn,J., Paarlberg,J., Kim,C.H., Munroe,D., Gangi,L., Han,J., Puri,R. *et al.* (2005) Three microarray platforms: an analysis of their concordance in profiling gene expression. *BMC Genomics*, **6**, 63.
7. Bammler,T., Beyer,R.P., Bhattacharya,D., Boorman,G.A., Boyles,A., Bradford,B.U., Bumgarner,R.E., Bushel,P.R., Chaturvedi,K., Choi,D.C. *et al.* (2005) Standardizing global gene expression analysis between laboratories and across platforms. *Nature Meth.*, **5**, 351–356.
8. Higuchi,R., Fockler,C., Dollinger,G. and Watson,R. (1993) Kinetic PCR analysis: real-time monitoring of DNA amplification reactions. *Biotechnology*, **9**, 1026–1030.
9. Larkin,J.E., Frank,B.C., Gavras,H., Sultana,R. and Quackenbush,J. (2005) Independence and reproducibility across microarray platforms. *Nature Meth.*, **5**, 337–343.
10. Liu,R.H., Yang,J., Lenigk,R., Bonano,J. and Grodzinski,P. (2004) Self-contained, fully integrated biochip for sample preparation, polymerase chain reaction amplification, and DNA microarray detection. *Anal. Chem.*, **76**, 1824–1831.
11. Lee,D.S., Park,S.H., Yang,H., Chung,K.H., Yoon,T.H., Kim,S.J., Kim,K. and Kim,Y.T. (2004) Bulk-micromachined submicroliter-volume PCR chip with very rapid thermal response and low power consumption. *Lab Chip*, **4**, 401–407.
12. Lagally,E.T., Medintz,I. and Mathies,R.A. (2001) Single-molecule DNA amplification and analysis in an integrated microfluidic device. *Anal. Chem.*, **3**, 565–570.
13. Nagai,H., Murakami,Y., Yokoyama,K. and Tamiya,E. (2001) High-throughput PCR in silicon based microchamber array. *Biosens. Bioelectron.*, **16**, 1015–1019.
14. Nagai,H., Murakami,Y., Morita,Y., Yokoyama,K. and Tamiya,E. (2001) Development of a microchamber array for picoliter PCR. *Anal. Chem.*, **73**, 1043–1047.
15. Matsubara,Y., Kerman,K., Kobayashi,M., Yamamura,S., Morita,Y. and Tamiya,E. (2004) On-chip nanoliter-volume multiplex TaqMan polymerase chain reaction from a single copy based on counting fluorescence released from microchambers. *Anal. Chem.*, **21**, 6434–6439.
16. Matsubara,Y., Kerman,K., Kobayashi,M., Yamamura,S., Morita,Y., Takamura,Y. and Tamiya,E. (2005) Microchamber array based DNA quantification and specific sequence detection from a single copy via PCR in nanoliter volumes. *Biosens. Bioelectron.*, **20**, 1482–1490.

17. Leamon,J.H., Lee,W.L., Tartaro,K.R., Lanza,J.R., Sarkis,G.J., de Winter,A.D., Berka,J., Weiner,M., Rothberg,J.M. and Lohman,K.L. (2003) A massively parallel PicoTiterPlate™ based platform for discrete picoliter-scale polymerase chain reactions. *Electrophoresis*, **24**, 3769–3777.
18. Silver,J., Mi,Z., Takamoto,K., Bunqay,P., Brown,J. and Powell,A. (1999) Controlled formation of low-volume liquid pillars between plates with a lattice of wetting patches by use of a second immiscible fluid. *J. Coll. Inter. Sci*., **219**, 81–89.
19. Daridon,A. (2005) Picofluidic digital PCR. In *Proceedings of the Conference on Quantitative PCR*. LaJolla, CA, USA.
20. Liu,J., Enzelberger,M. and Quake,S. (2003) A nanoliter rotary device for polymerase chain reaction. *Electrophoresis*, **23**, 1531–1536.
21. Marcus,J.S., Anderson,W.F. and Quake,S.R. (2006) Parallel picoliter RT–PCR assays using microfluidics. *Anal. Chem*., **78**, 956–958.
22. Kalinina,O., Lebedeva,I., Brown,J. and Silver,J. (1997) Nanoliter scale PCR with TaqMan detection. *Nucleic Acids Res*., **10**, 1999–2004.
23. Brown,J.F., Silver,J.E. and Kalinina,O.V. (2000) Method of sampling, amplifying and quantifying segment of nucleic acid, polymerase chain reaction assembly having nanoliter-sized sample chambers, and method of filling assembly. US Patent 6143496.
24. Brown,J.F., Silver,J.E. and Kalinina,O.V. (2002) Method of sampling, amplifying and quantifying segment of nucleic acid, polymerase chain reaction assembly having nanoliter-sized sample chambers, and method of filling assembly. US Patent 6391559 B1.
25. Brenan,C.J.H., Domansky,K., Kurzawski,P. and Griffth,L.G. (2000) BioMEMS applied to the development of cell-based bioassay systems. *SPIE Proceedings*, **3912**, 76–87.
26. Kanigan,T.K., Brenan,C.J.H., Lafontaine,S., Sosnowski,L., Madden,P.G. and Hunter,I.W. (2000) Living Chips for drug discovery. *SPIE Proceedings*, **3926**, 172–180.
27. Brenan,C.J.H., Morrison,T., Stone,K., Heitner,T., Katz,A., Kanigan,T.S. and Hess,R. (2002) A massively parallel microfluidics platform for storage and ultra high throughput screening. *SPIE Proceedings*, **4626**, 560–569.
28. Wang,X. and Seed,B. (2003) A PCR primer bank for quantitative gene expression analysis. *Nucleic Acids Res*., **31**, e154.
29. Ririe,K.M., Rasmussen,R.P. and Wittwer,C.T. (1997) Product differentiation by analysis of DNA melting curves during the polymerase chain reaction. *Anal. Biochem*., **245**, 154–160.
30. Lodish,H., Berk,A., Matsudaira,P., Kaiser,C.A., Krieger,M., Scott,M.P., Zipursky,S.L. and Darnell,J. (2004) *Molecular Cell Biology, 5th edn*. W.H. Freeman and Company, NY, pp. 304–307.
31. Robinson,M.O. and Simon,M.I. (1991) Determining transcript number using the polymerase chain-reaction: PGK-2, MP2 and PGK-2 transgene messenger-RNA levels during spermatogenesis. *Nucleic Acids Res*., **19**, 1557–1562.
32. Meagher,L., Mahiouz,D., Sugars,K., Burrows,N., Norris,P., Yarwood,H., Becker-Andre,M. and Haskard,D.O. (1994) Measurement of mRNA for E-selectin, VCAM-1 and ICAM-1 by reverse transcription and the polymerase chain reaction. *J. Immunol. Meth*., **175**, 237–246.
33. Kuldo,J., Westra,J., Asgeirsdottir,S.A., Kok,R.J., Oosterhuis,K., Rots,M.G., Schouten,J.P., Limburg,P.C. and Molema,G. (2005) Differential effects of NF-κB and p38 MAPK inhibitors and combinations thereof on TNF-α and IL-1β-induced proinflammatory status of endothelial cells *in vitro*. *Am. J. Physiol. Cell. Physiol*., **289**, C1229–C1239.